IET Generation, Transmission & Distribution

Special Issue on Power Electronic Converter Systems for Integration of Renewable Energy Sources

IET Journals
The Institution of Engineering and Technology

High-performance hybrid photovoltaic -battery system based on quasi-Z-source inverter: application in microgrids

ISSN 1751-8687
Received on 25th April 2014
Revised on 22nd April 2015
Accepted on 8th May 2015
doi: 10.1049/iet-gtd.2014.0336
www.ietdl.org

Jasem Khajesalehi, Keyhan Sheshyekani, Mohsen Hamzeh ✉, Ebrahim Afjei

Electrical and Computer Engineering Department, Shahid Beheshti University, G.C., Velenjak, Tehran 1983963113, Iran
✉ *E-mail: mo_hamzeh@sbu.ac.ir*

Abstract: This study presents a high-performance photovoltaic (PV)-battery hybrid power conversion system (HPCS) which is integrated to a microgrid using a quasi-Z-source inverter (qZSI). The battery system is directly connected to the intermediate dc link of the qZSI without any extra converter which reduces the size and the cost of the power electronic interface. A controller equipped with a harmonic compensator is designed to control the battery current in the grid-connected mode and to regulate the microgrid voltage in the islanded mode in the presence of unbalanced and non-linear loads. Furthermore, the proposed controller adjusts the shoot-through duty cycle of the qZSI to regulate the PV voltage to its reference value provided through the maximum power point tracking algorithm. Moreover, the proposed controller provides the microgrid with the capability to transfer between the two operation modes. A new strategy is adopted to keep the HPCS operational in case of severe reduction in the available power of the PV modules and its consequent voltage drop. The performance of the proposed control system is evaluated for the control of a typical microgrid simulated in MATLAB/SIMULINK environment.

1 Introduction

Photovoltaic (PV) systems are characterised by their variable power availability during different time scales. Owing to this fact, PV systems are equipped with energy storage systems, such as batteries, to store the excess of energy or supplement inadequate energy facilitating more seamless integration of PV systems with the grid [1]. The conventional architecture for the hybrid PV-battery system includes two dc/dc converters used for adapting different voltage ratings of the PV system and the battery as well as increasing the dc-link voltage to obtain the required output ac voltage [2]. Furthermore, the dc/dc converter in conventional voltage source inverters (VSIs) must regulate its output voltage so that the PV system operates at its maximum power point. This conversion system increases the size of the power circuit and the controller resulting in an expensive power electronic interface (PEI). To cope with these drawbacks of conventional PEIs, one can resort to Z-source inverters (ZSIs) which offer a single stage voltage conversion system with buck–boost capabilities [3]. This unique feature is obtained, thanks to the shoot-through duty cycle which is allowed in this type of inverters.

The quasi-ZSI (qZSI) has emerged as a more developed topology of ZSIs which draws a continuous current from the dc source so that there is no need for large filtering capacitors in the dc side [4]. It also reduces the voltage rating of one of the capacitors in the impedance network making it more suitable for distributed generation applications [5].

In [6–9], for increasing the boost capability and reducing the voltage stress across the devices, some more advanced topology of ZSI namely switched inductor ZSI, trans ZSI, extended boost Z-source family, asymmetric Γ-source inverter and so on, are proposed. In addition to the advanced types of ZSI, regarding the control of ZSI family, the maximum boost and the maximum constant boost control methods are proposed in [10, 11], respectively, where, both will decrease the voltage stress across the switches. Moreover, the maximum constant boost control method minimises the ripples on the current flowing through the inductors in the impedance network. In [12, 13], the average state space and the signal-flow graph methods have been used to model the dynamic and steady-state performance of ZSIs. In [14], for minimising the disturbance effects on the output voltage of the ZSI, a robust multi-loop control system has been designed based on the average state-space model of the ZSI impedance network. Moreover, in [15] a modified space vector pulse-width modulation (PWM) scheme has been proposed to regulate the ac-side voltage of the ZSIs. So far, the ZSIs have been used in many applications, such as renewable energy resources, uninterruptible power supplies, wind generation systems and active power filters [16–20].

Recently, the qZSI has been employed in a grid-tied application of a PV-battery system [21, 22]. In these structures, the battery is used to store redundant energy or supplement inadequate energy of the PV to reduce the fluctuations of the injected power to the grid. However, in view of emerging microgrid concept, the PV-battery system is required to have the capability to supply the required power when its host microgrid operates in both grid-connected and islanded modes of operation. In the latter mode, the PV-battery power conversion system must be able to regulate the microgrid voltage and supply the total – or a portion – of the load demand.

Within this context, in this paper, a new control strategy for a hybrid PV-battery power conversion system (HPCS) is proposed. The proposed HPCS is based on the qZSIs and works in both grid-connected and islanded modes of microgrid operation. In the islanded mode, the voltage of the microgrid is intended to be regulated, whereas in the grid-connected mode, the control system regulates the battery current and the power injected to the grid. A proportional resonant (PR) controller with harmonic compensator (HC) is employed to conduct the aforementioned control tasks particularly in the presence of unbalanced and non-linear loads [23, 24]. In the grid-connected mode, the battery current is regulated in both charging and discharging modes by adjustment of the inverter output current, whereas in the islanded mode, the battery current is determined by the load power demand. Moreover, the proposed control strategy maintains the voltage of the PV modules at its reference value to provide the maximum power point tracking (MPPT) in both microgrid modes of operation. Moreover, a new strategy is adopted to keep the HPCS operational in case of severe reduction in the available power of the PV modules and its consequent voltage drop. The performance of the proposed PV-battery HPCS and its control strategy is demonstrated through simulation studies conducted in the MATLAB/SIMULINK environment.

2 PV-battery HPCS

The proposed hybrid PV-battery HPCS employing the qZSI as PEI is shown in Fig. 1*a*. In this configuration, the battery and PV systems, with different voltage levels, are connected to the ac side with no need of any extra dc/dc converter stages. As a result, the overall installation cost, volume and losses are decreased in the proposed system. The battery system is connected in parallel with C_2. Since the voltage level of C_2 is small, a battery system with relatively lower voltage rating and cost as well as higher reliability and life-time can be used. Unlike the conventional VSIs, in the proposed system, the upper and lower switches of each phase leg can be turned on simultaneously which increases the reliability of the HPCS.

The dc side of the proposed system consists of two different ports namely the unidirectional and bidirectional ports. Moreover, a three-phase inverter is used between the impedance network and the ac side of the HPCS. The PV modules are connected to the inverter by the unidirectional port which forms a path through which the current flows from the PV modules to the impedance network. The battery system is connected to the intermediate dc link through a bidirectional port to operate in both charging and discharging modes. The protection relay disconnects the PV modules from the HPCS when the power of the PV system, and consequently its voltage, drops below a predefined value.

In the proposed configuration, the battery is connected in series with a small inductor to eliminate the high-frequency ripples on the battery current. To provide the required ac voltage, the qZSI utilises the shoot-through cycles between null vectors in the employed PWM algorithm to boost both the PV and the battery voltages to a desirable value to provide the required ac voltage.

To investigate the HPCS performance, the equivalent circuits of the qZSI in shoot-through and non-shoot-through conditions are shown in Figs. 1*b* and *c*. The three-phase inverter bridge and the external ac load are represented by a single switch S paralleled with a current source i_{load}. As the series inductor of the battery system is negligible compared with the inductors in the impedance network, we ignore it in system modelling. The voltage of the PV system is assumed to be v_P, whereas v_{b} denotes the battery voltage. The battery is modelled using a voltage source E_{b}, which is in series with a resistance R_{b} [25].

During the shoot-through state, switch S is closed and the reverse paralleled diode of the switch S' is inversely biased blocking the current to flow from the capacitors of the impedance network to the legs of the inverter. In non-shoot-through state, the switch S in Fig. 1*c* is open and the reverse paralleled diode of the switch S' conducts.

According to Figs. 1*b* and *c*, during the shoot-through state, the energy stored in C_2 is discharged in L_1 whereas in the non-shoot-through interval, the energy stored in L_2 is released in C_2 increasing its voltage. As a result, the energy which is exchanged between C_2 and the impedance network takes place in a bidirectional manner providing C_2 with the capability of charging and discharging the battery unit.

Considering capacitor voltages and inductor currents as the state space variables $\boldsymbol{x} = \left[i_{L_1}\ i_{L_2}\ v_{C_1}\ v_{\text{b}}\right]^{\text{T}}$, in the shoot-through duration, the state-space equation can be obtained as

$$\boldsymbol{F}.\frac{\mathrm{d}\boldsymbol{x}}{\mathrm{d}t} = \boldsymbol{A}_{\text{st}} \cdot \boldsymbol{x} + \boldsymbol{B}_{\text{st0}} \cdot \boldsymbol{u}_0 \tag{1}$$

where

$$\boldsymbol{u}_0 = \begin{bmatrix} v_{\text{p}} \\ i_{\text{load}} \\ E_{\text{b}} \end{bmatrix}, \quad \boldsymbol{A}_{\text{st}} = \begin{bmatrix} -r_1 & 0 & 0 & 1 \\ 0 & -r_2 & 1 & 0 \\ 0 & -1 & 0 & 0 \\ -R_{\text{b}} & 0 & 0 & -1 \end{bmatrix}$$

$$\boldsymbol{B}_{\text{st0}} = \begin{bmatrix} 1 & 0 & 0 \\ 0 & 0 & 0 \\ 0 & 0 & 0 \\ 0 & 0 & 1 \end{bmatrix} \text{ and } \boldsymbol{F} = \text{diag}(L_1\ L_2\ C_1\ R_{\text{b}} \cdot C_2)^{\text{T}}$$

Similarly, the state-space model of the system in the

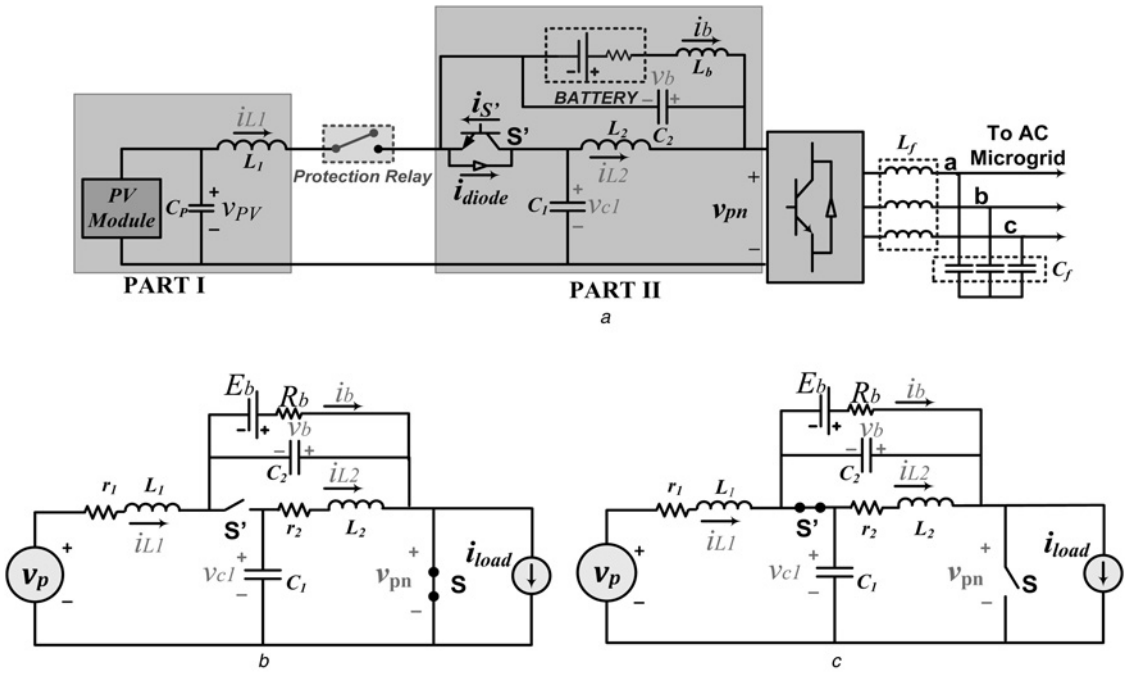

Fig. 1 *Proposed PV-battery HPCS*

a Structure of the proposed system for the microgrid application
b Equivalent circuit of the proposed system during shoot-through
c Non-shoot-through condition

IET Gener. Transm. Distrib., 2015, Vol. 9, Iss. 10, pp. 895–902

non-shoot-through condition is obtained as

$$\boldsymbol{F}\cdot\frac{\mathrm{d}\boldsymbol{x}}{\mathrm{d}t}=\boldsymbol{A}_{\mathrm{nst}}\cdot\boldsymbol{x}+\boldsymbol{B}_{\mathrm{nst0}}\cdot\boldsymbol{u}_0 \tag{2}$$

where

$$\boldsymbol{A}_{\mathrm{nst}}=\begin{bmatrix}-r_1 & 0 & -1 & 0\\ 0 & -r_2 & 0 & -1\\ 1 & 0 & 0 & 0\\ 0 & R_{\mathrm{b}} & 0 & -1\end{bmatrix},\quad \boldsymbol{B}_{\mathrm{nst0}}=\begin{bmatrix}1 & 0 & 0\\ 0 & 0 & 0\\ 0 & -1 & 0\\ 0 & -R_{\mathrm{b}} & 1\end{bmatrix}$$

Using average state method, the system average state-space equations can be written as

$$\boldsymbol{F}\cdot\frac{\mathrm{d}\boldsymbol{x}}{\mathrm{d}t}=\boldsymbol{A}\cdot\boldsymbol{x}+\boldsymbol{B}_0\cdot\boldsymbol{u}_0,\quad \boldsymbol{y}=\boldsymbol{C}\cdot\boldsymbol{x}+\begin{bmatrix}0 & E_{\mathrm{b}}/R_{\mathrm{b}}\end{bmatrix}^{\mathrm{T}} \tag{3}$$

where

$$\boldsymbol{A}=d\cdot\boldsymbol{A}_{\mathrm{st}}+(1-d)\cdot\boldsymbol{A}_{\mathrm{nst}},\quad \boldsymbol{B}_0=d\cdot\boldsymbol{B}_{\mathrm{st0}}+(1-d)\cdot\boldsymbol{B}_{\mathrm{nst0}}$$

$$\boldsymbol{y}=\begin{bmatrix}i_{L_1} & i_{\mathrm{b}}\end{bmatrix}^{\mathrm{T}},\quad \boldsymbol{C}=\begin{bmatrix}1 & 0 & 0 & 0\\ 0 & 0 & 0 & -1/R_{\mathrm{b}}\end{bmatrix}$$

and d represents the shoot-through duty cycle of the inverter.

To obtain the small-signal model of the system, perturbations $\hat{d}$ and $\hat{i}_{\mathrm{load}}$ are associated to d and i_{load}, respectively, which in turn result in variations $\hat{i}_{\mathrm{b}}$ and $\hat{\boldsymbol{x}}=\begin{bmatrix}\hat{i}_{L_1} & \hat{i}_{L_2} & \hat{v}_{C_1} & \hat{v}_{\mathrm{b}}\end{bmatrix}$ in i_{b} and $\boldsymbol{x}$. The small-signal model of (3) can be obtained as

$$\boldsymbol{F}\cdot\frac{\mathrm{d}\hat{\boldsymbol{x}}}{\mathrm{d}t}=\boldsymbol{A}\cdot\hat{\boldsymbol{x}}+\boldsymbol{B}\cdot\hat{\boldsymbol{u}},\quad \hat{\boldsymbol{y}}=\boldsymbol{C}\cdot\hat{\boldsymbol{x}} \tag{4}$$

where

$$\boldsymbol{B}=\begin{bmatrix}0 & V_{11}\\ 0 & V_{11}\\ D-1 & I_{11}\\ 1-D & -I_{11}\end{bmatrix},\quad \hat{\boldsymbol{u}}=\begin{bmatrix}\hat{i}_{\mathrm{load}} & \hat{d}\end{bmatrix}\ \text{and}\ \hat{\boldsymbol{y}}=\begin{bmatrix}\hat{i}_{L_1} & \hat{i}_{\mathrm{b}}\end{bmatrix}^{\mathrm{T}}$$

In (4), all variables denote the small-signal perturbation around the operating point. Moreover, D, V_{C_1}, I_{L_1}, I_{b} and I_{load} represent the shoot-through duty cycle, voltage of C_1, the current of L_1, the battery current and the load current in steady state, whereas $V_{11}=V_{C_1}-R_{\mathrm{b}}I_{\mathrm{b}}+E_{\mathrm{b}}$ and $I_{11}=I_{\mathrm{load}}-2I_{L_1}+I_{\mathrm{b}}$. By neglecting the parasitic resistance of inductors, in steady-state condition, the left side of (3) is zero and the following equations are obtained

$$V_{\mathrm{b}}=\frac{D}{1-2D}V_{\mathrm{p}} \tag{5}$$

$$V_{\mathrm{pn}}=\frac{1}{D}V_{\mathrm{b}} \tag{6}$$

where V_{b}, V_{p} and V_{pn}, respectively, represent the battery voltage, the PV voltage and the inverter dc-link peak voltage. The amplitude of the fundamental component of the voltage in the ac side of the inverter (v_{inv}) is obtained as

$$v_{\mathrm{inv}}=m\frac{v_{\mathrm{pn}}}{2} \tag{7}$$

where m denotes the inverter modulation index.

Referring to (5)–(7), there are two parameters m and D, which can be used separately to regulate the ac-side voltage of the inverter and the voltage of the PV system in grid-connected and islanded modes. In the proposed control strategy in both grid-connected and islanded modes of operation, the shoot-through duty cycle of the inverter d is used to control the voltage of the PV module, whereas the inverter modulation index is used to regulate the inverter ac-side current. According to the state-space model of the system in (4) and considering that the average voltage across the inductors and average current of capacitors are zero at steady state and also ignoring the second-order elements, the system transfer functions are obtained as

$$G_{\hat{i}_{\mathrm{load}}}^{\hat{i}_{\mathrm{b}}}=\frac{(1-D)(Ls+r)}{R_{\mathrm{b}}LCs^2+(rR_{\mathrm{b}}C+LD)s+rD+(2D-1)^2R_{\mathrm{b}}} \tag{8}$$

$$G_{\hat{d}}^{\hat{i}_{L_1}}=\frac{R_{\mathrm{b}}CV_{11}s+DV_{11}+R_{\mathrm{b}}I_{11}(2D-1)}{R_{\mathrm{b}}LCs^2+(rR_{\mathrm{b}}C+LD)s+rD+(2D-1)^2R_{\mathrm{b}}} \tag{9}$$

Note that in (8) and (9), it is assumed that $r=r_1=r_2$, $C=C_1=C_2$ and $L=L_1=L_2$.

3 Description of the proposed control strategy

We consider the proposed PV-battery HPCS in a microgrid with the capability to operate in both grid-connected and islanded modes. Normally, the microgrid operates in the grid-connected mode and the HPCS regulates the injected power to the grid. Moreover, in islanded mode, HPCS is controlled to maintain the voltage and frequency within the allowable limits. Note that islanded operation might be initiated either intentionally (such as maintenance or economic reasons) or when a fault occurs in the main grid.

The proposed control strategy for both modes of operation is shown in Fig. 2*a*. In the grid-connected mode, the selector switch is in state 'B' and the controller regulates the battery current or adjusts the active and reactive power injections to the grid. In this mode, the inverter current ($i_{L_{\mathrm{f}}}$) is controlled either by the battery current controller or the power controller. For transferring to the islanded mode, the selector switch is changed to state 'A' and the inverter reference current is provided by the microgrid voltage controller.

In both modes of HPCS operation, the voltage of the PV system is dedicated by the MPPT algorithm [26]. As shown in Fig. 2*a*, the inverter output current is regulated by adjusting the inverter modulation index, whereas the shoot-through duty cycle of the inverter is used to regulate the PV voltage to its MPPT reference. These distinct roles of the modulation index and the shoot-through duty cycle provide the proposed controller with the capability of adjusting the PV voltage to its reference value regardless of the microgrid operation mode.

Fig. 2*b* demonstrates the structure of the multifunctional controller for the proposed PV-battery HPCS. The controller is divided into four control units namely (i) ac current controller, (ii) battery current controller, (iii) ac voltage controller and (iv) PV voltage controller. It is noted that the three first controllers are dependent on each other, whereas the PV voltage controller is independent from the other control units. The measured currents and voltages in ac side are transferred to $\alpha\beta$ stationary reference frame. To effectively control the output voltage and the current of the qZSI in $\alpha\beta$ stationary reference frame, the proportional resonance (PR) controller with HC is used [24]. The PR–HC controller enables the HPCS to supply the negative-sequence and the harmonic components of the unbalanced and non-linear loads in the islanded microgrid.

To design the controller, first, the ac current controller is designed as the inner controller for the ac voltage controller and the battery current controller. In the next step, the ac voltage controller and the battery current controller are designed. Finally, the PV voltage controller is designed as an independent controller. The HPCS parameters and the steady-state variables used in the qZSI modelling are listed in Table 1.

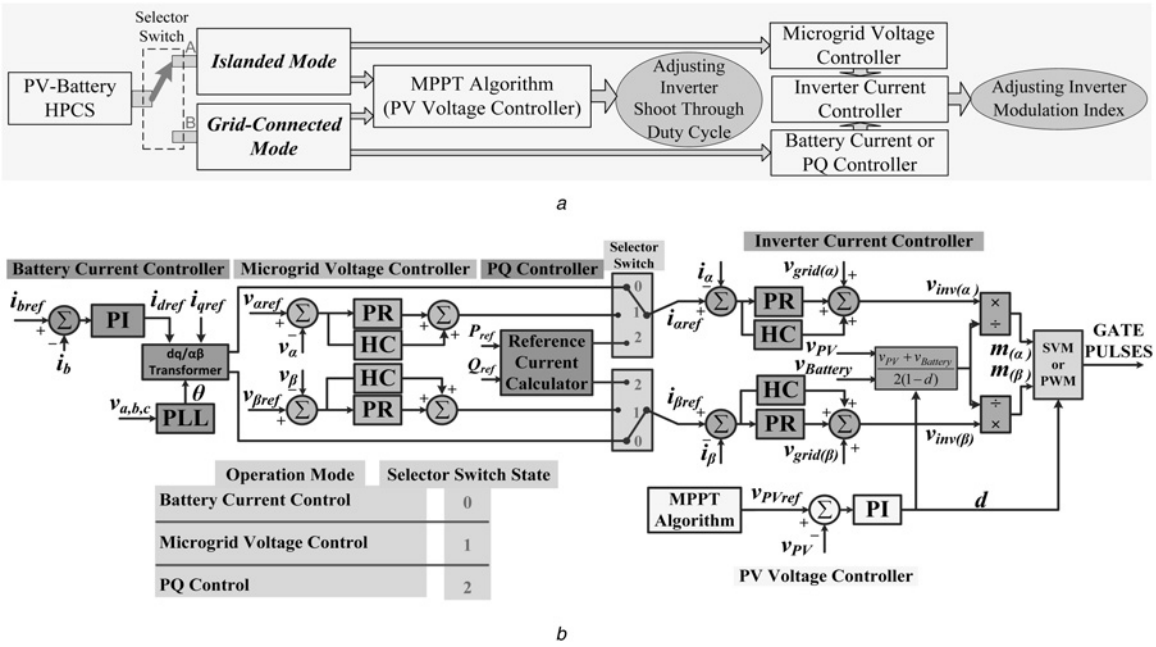

Fig. 2 *Proposed control system for the PV-battery HPCS used in microgrid*

a Flowchart
b Overall structure

3.1 AC current controller

As it is shown in Figs. 2*a* and *b*, in the grid-connected mode, the inverter current controller has a significant role to control the exchanged real and reactive power between the grid and the HPCS. In the islanded mode, the inverter current controller is used as an inner loop to actively damp the resonance of the inverter inductive-capacitance filter. The transfer functions of the PR and the HC compensators used in the inverter current controller are as follows

$$\mathrm{PR} = K_{\mathrm{P}} + \frac{K_R s}{s^2 + \zeta s + \omega^2} \tag{10}$$

$$\mathrm{HC} = \sum_{n=5,7,11} \frac{K_{Rn} s}{s^2 + \zeta s + (n\omega)^2} \tag{11}$$

where ω (rad/s) is the nominal frequency and ζ is used to limit the controller gain at system nominal frequency. In this paper, the HC is intended to compensate the 5th, 7th and 11th harmonic components. As shown in Fig. 2*b*, in the grid-connected mode, a feed-forward of the grid voltage is utilised to eliminate the effect of the grid voltage disturbances on the current controller, whereas in the islanded mode the feed-forward loop is bypassed.

According to (7), the inverter voltage (v_{inv}) depends on the inverter dc-link peak voltage (v_{pn}). To eliminate the effect of the impedance network disturbance on the ac-side current controller, the inverter voltage reference provided by the current controller is divided by $v_{\mathrm{pn}}/2$, as shown in Fig. 2*b*. The inverter dc-side voltage is a pulsed-shape voltage denoted by v_{pn} in non-shoot-through condition, while takes a zero value in shoot-through condition. Hence, it is not practical to directly measure the inverter dc-link peak voltage. Instead, this voltage is calculated using state-space model of the system expressed by (3)

$$v_{\mathrm{pn}} = (v_{\mathrm{pv}} + v_{\mathrm{bat}})/(1 - d) \tag{12}$$

Referring to (12), the calculation of the v_{pn} needs the measurement of both PV and battery voltages. Moreover, the value of the shoot-through duty cycle for calculation of v_{pn} is provided by the PV voltage controller.

The ac-side model of the system in Laplace domain is shown in Fig. 3*a*. To design a current controller characterised by a

Table 1 PV-battery HPCS parameters

Parameters	Values
quasi-Z-source inductances (L_1 and L_2)	600 μH
inductances parasitic resistance (r_1 and r_2)	0.1 Ω
quasi-Z-source capacitances (C_1 and C_2)	600 μF
AC side inductances (L_{f})	2 mH
parasitic resistance of L_{f}, (r_{f})	0.1 Ω
AC side inductance (C_{f})	25 μF
battery equivalent resistance (R_{b})	0.2 Ω
V_{11}	600 V
I_{11}	−75 A
D	0.33

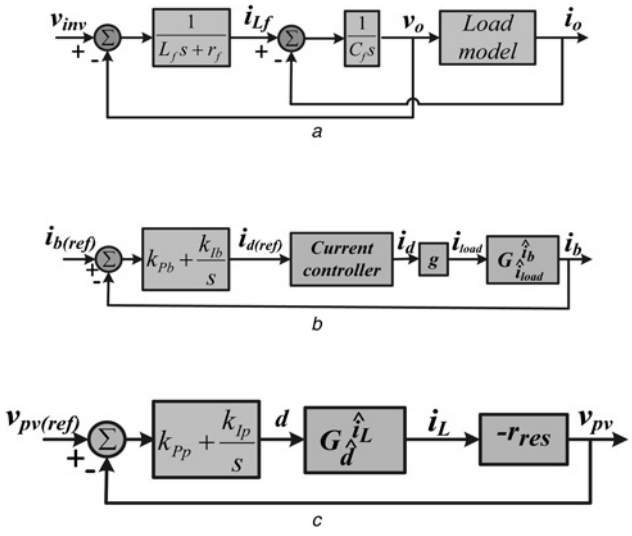

Fig. 3 *Model system in Laplace domain*

a AC side model of the inverter
b Battery current controller model
c PV voltage controller model

Table 2 PR controller coefficients

current controller	K_{PC}, K_{RC}	1.5, 4000
	K_{RC5}, K_{RC7}, K_{RC11}	1000, 1000, 1000
voltage controller	K_{PC}, K_{RC}	0.35, 400
	K_{RC5}, K_{RC7}, K_{RC11}	32, 80, 44

bandwidth (BW) of 1 kHz and a phase margin of 63°, we select the current controller parameters as listed in Table 2.

3.2 Battery current controller

In the grid-connected mode, the battery current is adjusted to charge the battery to a certain state of charge. The battery current controller produces the directional reference component of current (i_d), whereas the quadratic component (i_q) is set to zero. The block diagram of the battery system model is shown in Fig. 3*b*. In this model, $G_{i_{load}}^{\hat{i}_b}$ is calculated from (8). For a particular value of modulation index and shoot-through duty cycle, the value of i_{load} is proportional to i_d, Fig. 3*b*. It is noted that the BW of the battery current control system is considered lower than the BW of the inner ac current controller. The design choice of $k_{Pb} = 0.1$ and $k_{Ib} = 100$ for the battery current controller leads to a BW of 18 Hz and a phase margin of 100° as shown in Fig. 4.

3.3 AC voltage controller

In the islanded mode, the selector switch in Fig. 2*b* transfers to the ac voltage control mode (state '1') and the reference currents ($i_{\alpha\beta(ref)}$) are produced by the ac voltage controller. The ac voltage controller utilises the PR controller and the HC to regulate the HPCS output voltage in the presence of unbalanced and non-linear loads. The non-linear and unbalanced loads absorb oscillatory power from the HPCS that imposes a low-frequency ripple on the dc-link voltage. As discussed earlier, in the proposed control strategy, the output of the current controller is divided by the dc-link peak voltage which decreases the total harmonic distortion of the microgrid voltage. The coefficients of the PR voltage controller are listed in Table 2.

3.4 PV voltage controller

The PV voltage controller model in Laplace domain is shown in Fig. 3*c*. The PV voltage controller is designed based on the model described in (9). The residual resistor r_{res} is the equivalent resistance of the PV system in a given operating point.

In the grid-connected mode, the selector switch is in the battery current control mode. Owing to the constant power injection to the grid, the increase/decrease in the PV power, initially, leads to a decrease/increase in the battery current. Subsequently, the battery current controller reacts and increases/decrease the injected power to the grid by controlling i_d to maintain the battery current at its charging or discharging reference.

In the islanded mode of operation, the output power of the HPCS is equal to the load demand. In this mode, the inverter ac current is regulated by the voltage controller. Thus, any increase in the PV power leads to a reduction in the battery current. Considering $r_{res} = 3\ \Omega$, the design choice of $k_{Pp} = -2.5 \times 10^{-4}$ and $k_{Ip} = -0.1$ for the PV voltage controller, provides a BW and a phase margin of 128 Hz and 83°, respectively, as shown in Fig. 4.

4 Operation of the proposed system during the reduction of available power of the PV system

As it can be seen from (5), in case of reduction of the available power of the PV system and its consequent voltage drop, D must be increased to adapt PV and battery voltages. Following the required increase in D, the dc-link voltage is decreased according to (6).

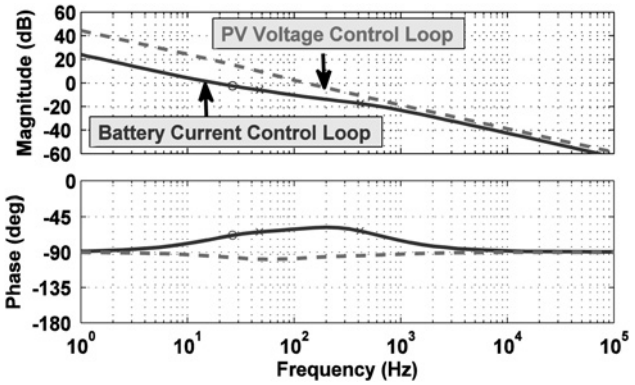

Fig. 4 *Bode plots of the battery current and PV voltage controllers*

Hence, from (7), the ac-side voltage of the inverter is decreased too. The reduction of the inverter voltage leads to an increase in m which is provided by the current controller. Owing to the single-stage power conversion structure of the qZSI, D and m are dependent on each other. This means that the boost capability of the qZSI is achieved by partially or fully replacing conventional null switching vectors of (0 0 0) and (1 1 1) with shoot-through state [3]. Therefore for proper operation of qZSI PWM, (13) has to be fulfiled in the method used in this paper

$$M < 1 - D \tag{13}$$

where M is the inverter modulation index in the steady state. Referring to (13) and (7), we have

$$V_{inv} < \frac{1 - D}{2} V_{pn} \tag{14}$$

where V_{inv} represents the peak value of inverter phase-to-null voltage in ac side (v_{inv}) in the steady state. The value of D for adjusting the PV and battery voltages in steady state can be obtained from (5). Substituting D from (5) into (14) and referring to (6), the proper operating condition of the system is as follows

$$V_{PV} > 2V_{inv} - V_{bat} \tag{15}$$

Therefore the PV voltage is not allowed to drop lower than the minimum value expressed by (15). In case that the PV voltage violates from its minimum allowable value, the PV system (i.e. Part I in Fig. 1*a*) is disconnected from the system by means of the protection relay. In this condition, the battery system (i.e. Part II in Fig. 1*a*) individually provides the power demand. As shown in Fig. 1, in this condition, when the inverter is in shoot-through state, the switch S is 'on' and the reverse paralleled diode in the switch S' is reversely biased. The voltage across L_2 is $+v_{C_1}$ that increases the energy stored in the inductor. In non-shoot-through state, the switch S is 'off' and the load current is supplied by the impedance network. Assuming that the paralleled diode of S' is directly biased, the voltage across L_2 is $-v_b$ that discharges the energy stored in L_2. In this condition, the current flowing through the paralleled diode of S' in Fig. 1*a* is

$$i_{diode} = -i_{L_2(0)} + \left(\frac{v_b}{L_2}\right)t + i_{load} \tag{16}$$

where $i_{L_2(0)}$ is the initial current of L_2 in non-shoot-through state. In duration that the paralleled diode conducts ($i_{diode} > 0$), v_{pn} is equal to $v_{C_1} + v_b$ which is desirable for transferring power from the dc side to the ac side. However, when i_{diode} in (16) reaches to zero, the paralleled diode is unwantedly reversely biased. Assuming a constant value for load current in non-shoot-through state, the inductor current i_{L_2} becomes equal to the load current i_{load} (see

Table 3 System specifications

Parameters	Value
microgrid voltage (phase-null)	120 $V_{(RMS)}$
microgrid frequency	60 Hz
battery no-load voltage	200 V
switching frequency (f_s)	10 kHz
battery series inductor (L_b)	40 μH
PV capacitor (C_P)	50 μF

Fig. 1*b*). Therefore voltage across L_2 is zero and v_{pn} equals v_{C_1}. Hence, the dc-link peak voltage varies between v_{C_1} and $v_{C_1} + v_b$ resulting in the interruption of power transferring from the dc side to the ac side. To cope with this issue, the switch S' must receive gate pulses to be turned on in non-shoot-through state and to be turned off in shoot-through state. In doing so, v_{pn} remains equal to $v_{C_1} + v_b$ in non-shoot-through state providing the required voltage level for the power transfer. Note that when the PV is disconnected, the shoot-through duty cycle of the inverter is set to a constant value resulting in a value of V_{pn} which is appropriate for the power transfer. Since the battery has a constant output voltage, the inverter shoot-through duty cycle can be reasonably produced in an open-loop manner. Moreover, as the PV gets disconnected, it is not possible to estimate the dc-link peak voltage by (5). Hence, according to (6), the dc-link peak voltage is set to a constant value of V_{bat}/D.

5 Simulation results

The operation of the proposed HPCS in the grid-connected and islanded modes as well as during the transition between them is investigated through simulation studies conducted in the MATLAB/SIMULINK environment. The system specifications and controllers' parameters are listed in Tables 1–3.

The performance of the proposed system is studied for different case studies. First, the grid-connected operation of the PV-battery HPCS is investigated. Then, the islanded mode of operation in the presence of unbalanced and non-linear loads is investigated. The performance of the proposed control system during the transition from the islanded mode to the grid connected mode and vice versa is discussed. Finally, the efficiency of the system subject to an excessive voltage drop of the PV is investigated.

5.1 Grid-connected mode

In the grid-connected mode of microgrid operation, the battery charging current reference is initially set to 30 A, while at $t = 0.1$ s, the battery current reference is changed to discharging current of 5 A. At $t = 0.2$ s, the battery current reference is again changed to the charging current of 30 A. Moreover, the PV voltage is set to 200 V generating 5 kW power. As shown in Fig. 5*a*, the battery current controller manages to regulate the battery current to its reference both in charging and discharging modes. As shown in Fig. 5*b*, the increase of the battery current reference leads to the increase in the current injected to the grid. Moreover, as can be seen in Fig. 5*c*, despite the severe variation in battery current reference, the PV voltage is kept around its reference. The output power of the battery, the PV and the HPCS is shown in Fig. 5*d*. As seen from this figure, when the battery power is negative; the hybrid system absorbs power from the grid behaving like a consuming load. In duration that the battery power is positive, the HPCS injects power to the grid operating as a generator.

To evaluate the effectiveness of the PV voltage controller, different step changes in the PV reference voltage are considered as shown in Fig. 6*a*. The PV voltage controller tracks the reference provided by the MPPT algorithm. The battery is supposed to draw a charging current of 20 A. As shown in Fig. 6*b*, during the considered voltage variation, the battery current is kept constant equal to the reference value.

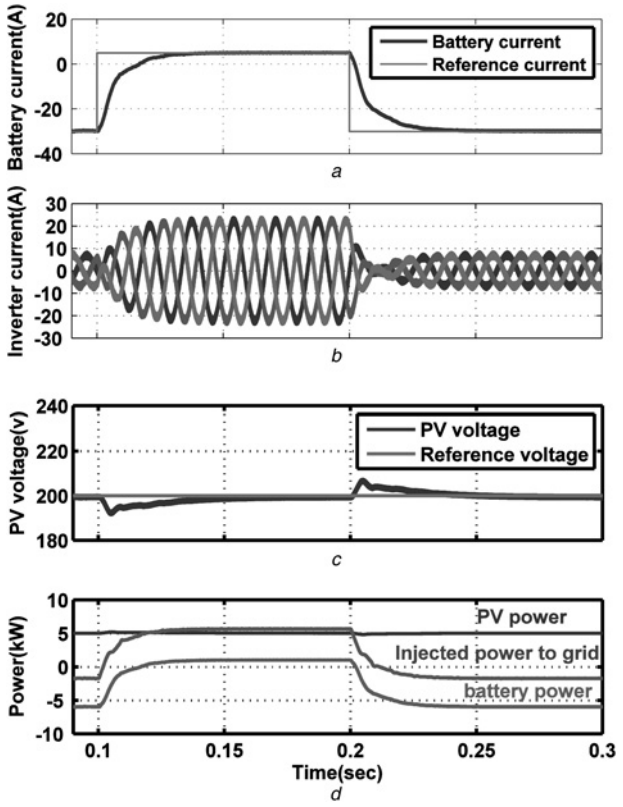

Fig. 5 *Variation of the battery current reference in grid-connected mode*

a Battery current
b Inverter output current
c PV voltage
d HPCS powers

5.2 Islanded mode

In the islanded mode of operation, the reference of the ac current controller in stationary reference frame is provided by the ac voltage controller. It is noted that since the PV has variable power availability, the battery current is inherently regulated in such a way to keep the balance between the load demand and the supply. The PV voltage is set to 200 V generating 10 kW power, and the ac voltage controller regulates the phase voltage of the microgrid to 120 $V_{(RMS)}$, 60 Hz.

At first, a 5 kW load is connected to the microgrid at $t = 0.07$ s and the total load power is increased to 10 kW. Subsequently, at $t = 0.13$ s, a single phase load with 2.8 kW is connected to phase-a. Finally at

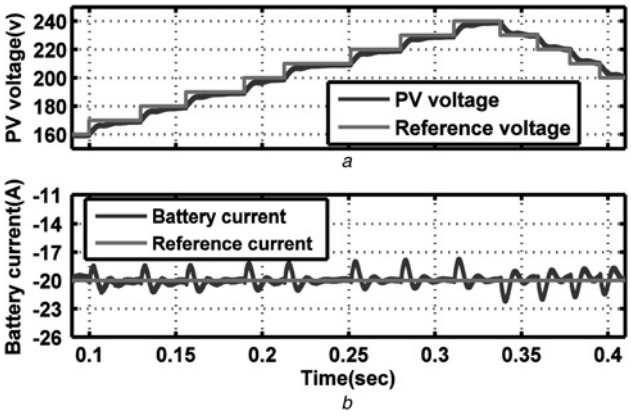

Fig. 6 *Evaluation of the effectiveness of the PV voltage controller*

a PV voltage variation
b Battery current during reference change of PV voltage controller

IET Gener. Transm. Distrib., 2015, Vol. 9, Iss. 10, pp. 895–902

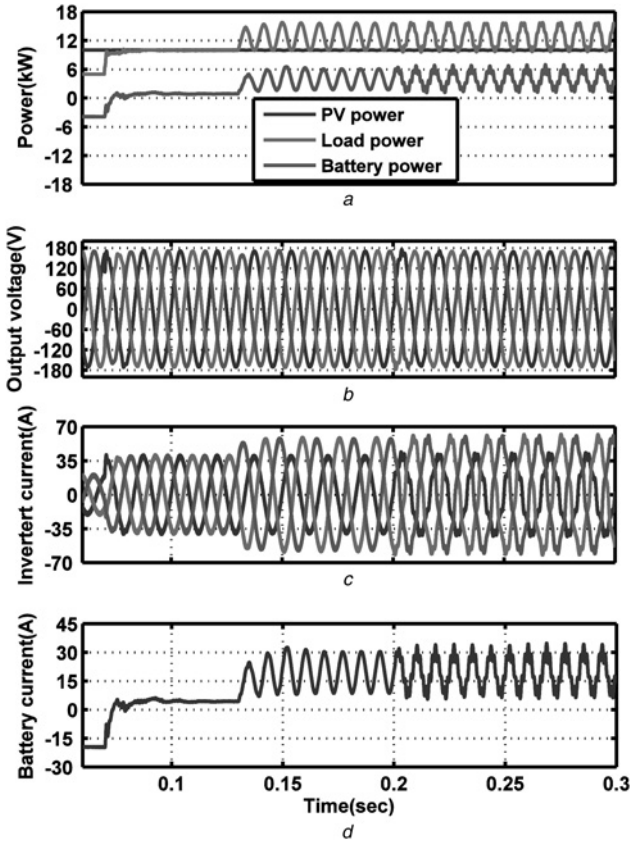

Fig. 7 *Microgrid voltage regulation during load changes*

a Microgrid load and HPCS powers
b Load voltage
c Load current
d Battery current

$t = 0.2$ s, a three-phase non-linear load is connected to the microgrid. The power of the microgrid load and the HPCS components during the considered load switchings are depicted in Fig. 7*a*. As can be seen in this figure, the load power variations make the battery power vary accordingly to supply the load power demand, while the PV power is constant.

The inverter voltage and the current during the load variations are shown in Figs. 7*b* and *c*, respectively. As it can be seen in Fig. 7*c*, the inverter current became unbalanced at $t = 0.13$ s, whereas the PR controller keeps the load voltage balanced. According to Fig. 7*c* at $t = 0.2$ s, the load current is contaminated with harmonics, whereas the voltage harmonic distortion is negligible.

The battery current during the load variations is shown in Fig. 7*d*. Following the load change at $t = 0.07$ s, the battery current is increased to keep the balance between the load demand and the supply. At $t = 0.13$ s, the load becomes unbalanced resulting in oscillations in the battery current. Subsequent to the connection of the non-linear load at $t = 0.2$ s, harmonic currents are drawn from the qZSI. The unbalanced and harmonic components of the load current make the battery current distorted as shown in Fig. 7*d*.

In the islanded mode, the performance of the proposed control system for finding the maximum power point is shown in Fig. 8*a*. In this mode, the load demand must be supplied by both the PV and the battery. Hence, the battery current changes such that the load demand is supplied, Fig. 8*b*. As can be seen in Fig. 8*c*, the ac voltage is not affected by the variations in the dc-side voltage.

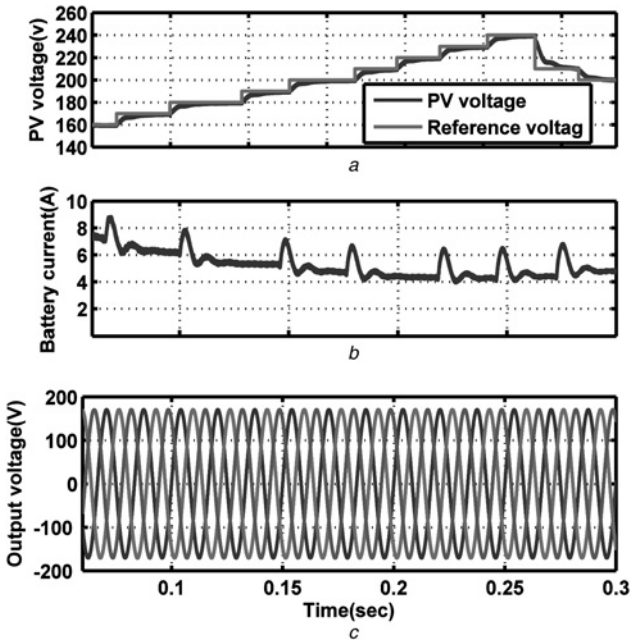

Fig. 8 *MPPT algorithm*

a PV voltage
b Battery current
c Microgrid voltage

5.3 Transfer mode

We first consider that the microgrid operates in the grid-connected mode and the battery is charged by a charging current of 30 A, while the PV voltage is maintained at 200 V by the associated controller. Moreover, the total load power of microgrid is 6 kW while the PV power generation is about 3.3 kW. Subsequent to disconnection from the main grid at $t = 0.1$ s, the HPCS takes over

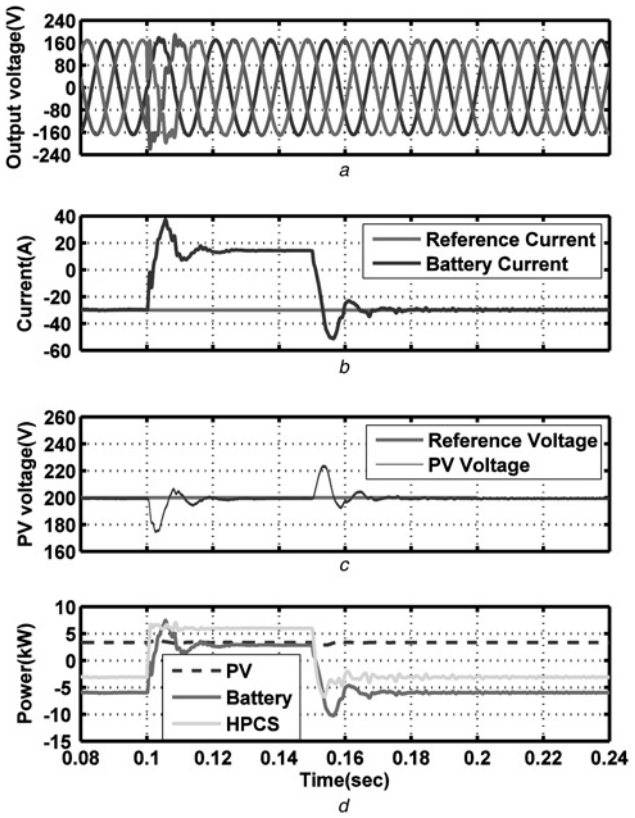

Fig. 9 *PV-battery HPCS performance during transfer modes*

a Microgrid voltage
b Battery current
c PV voltage
d Output power of the HPCS, the PV system and the battery system

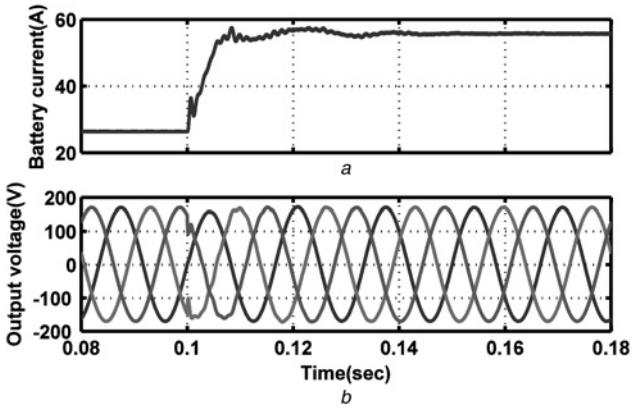

Fig. 10 *System operation in case of PV voltage drop*

a Battery current
b Microgrid voltage

the responsibility of regulating the microgrid voltage. At $t = 0.15$ s, the microgrid is reconnected to the grid and the battery current is brought back to its reference value of −30 A. The load voltage during these transitions is shown in Fig. 9*a*. It can be seen from this figure that the microgrid voltage experiences a smooth transition when the operation mode is changed. As shown in Fig. 9*b*, the battery current takes a different value from its reference to keep the balance between the supply and the demand. As shown in Fig. 9*c*, the PV voltage is kept to its reference despite the severe variation in the battery current from −30 to +14 A. The output power of the HPCS, the PV system and the battery system are shown in Fig. 9*d*. The PV power is 3.3 kW in both modes of the microgrid. However, the battery power changes from −6 to 2.7 kW for the grid-connected and islanded mode, respectively. In the grid-connected mode, the hybrid system absorbs 2.7 kW from the grid, whereas in the islanded mode, 6 kW power is injected to the loads.

5.4 PV voltage drop condition

It is assumed that the HPCS supplies a 5 kW load in islanded mode, although a voltage drop has occurred. Thus, the PV system is disconnected by the protection relay as described in Section 4. At $t = 0.1$ s, a 5 kW load is added to the microgrid. In this condition, the battery supplies the load demand. As it can be seen in Fig. 10*a*, the increase in load demand leads to appropriate increase in the battery current. The sinusoidal voltage of the microgrid shown in Fig. 10*b* confirms the effectiveness of the proposed control system when the PV system is disconnected from the HPCS.

6 Conclusion

A control scheme for the PV-battery HPCS based on the qZSI has been proposed. The qZSI uses single-stage buck–boost voltage conversion system which reduces the total cost and size of the PEI of the HPCS compared with the conventional systems. The microgrid application of the PV-battery HPCS has been investigated for both grid-connected and islanded modes of operation as well as during the transition between them. A new strategy was adopted to keep the HPCS operational in case of severe reduction in the available power of the PV modules and its consequent voltage drop. The performance of the proposed system has been evaluated in the presence of unbalanced and non-linear loads. It has been shown that the proposed system provides an acceptable performance for the microgrids in both grid-connected and islanded modes of operation and transition between them.

7 References

1 Riffonneau, Y., Bacha, S., Barruel, F., Ploix, S.: 'Optimal power flow management for grid-connected PV systems with batteries', *IEEE Trans. Sustain. Energy*, 2011, **2**, (3), pp. 309–320
2 Fakham, H., Lu, D., Francois, B.: 'Power control design of a battery charger in a hybrid active PV generator for load-following applications', *IEEE Trans. Ind. Electron.*, 2011, **58**, (1), pp. 85–94
3 Peng, F.Z.: 'Z-source inverter', *IEEE Trans. Ind. Appl.*, 2003, **39**, pp. 504–510
4 Anderson, J., Peng, F.Z.: 'Four quasi-Z-source inverters'. Proc. IEEE PESC'08, June 2008, pp. 2743–2749
5 Li, Y., Jiang, S., Cintron-Rivera, J.G., Peng, F.Z.: 'Modeling and control of quasi-Z-source inverter for distributed generation applications', *IEEE Trans. Ind. Electron.*, 2013, **60**, pp. 1532–1541
6 Zhu, M., Yu, K., Luo, F.L.: 'Switched inductor Z-source inverter', *IEEE Trans. Power Electron.*, 2010, **25**, (8), pp. 2150–2158
7 Qian, W., Peng, F.Z., Cha, H.: 'Trans-Z-source inverters', *IEEE Trans. Power Electron.*, 2011, **26**, (12), pp. 3453–3463
8 Gajanayake, C.J., Lin, L.F., Hoay, G., Lam, S.P., Kian, S.L.: 'Extended boost Z-source inverters', *IEEE Trans. Power Electron.*, 2010, **25**, (10), pp. 2642–2652
9 Mo, W., Loh, P.C., Blaabjerg, F.: 'Asymmetrical Γ-Source inverters', *IEEE Trans. Ind. Electron.*, 2014, **61**, (2), pp. 637–647
10 Peng, F.Z., Shen, M., Qian, Z.: 'Maximum boost control of the *Z*-source inverter', *IEEE Trans. Power Electron.*, 2005, **20**, (4), pp. 833–838
11 Shen, M., Wang, J., Joseph, A., Peng, F.Z.: 'Constant boost control of the Z-source inverter to minimize current ripple and voltage stress', *IEEE Trans. Ind. Appl.*, 2006, **42**, (3), pp. 770–778
12 Loh, P.C., Vilathgamuwa, D.M., Gajanayake, C.J., Lim, Y.R., Teo, C.W.: 'Transient modeling and analysis of pulse-width modulated Z-source inverter', *IEEE Trans. Power Electron.*, 2007, **22**, (2), pp. 498–507
13 Liu, J.B., Hu, J.G., Xu, L.Y.: 'Dynamic modeling and analysis of Z-source converter – derivation of AC small signal model and designoriented analysis', *IEEE Trans. Power Electron.*, 2007, **22**, (5), pp. 1786–1796
14 Gajanayake, C.J., Vilathgamuwa, D.M., Loh, P.C.: 'Development of a comprehensive model and a multiloop controller for Z-source inverter DG systems', *IEEE Trans. Ind. Electron.*, 2007, **54**, (4), pp. 2352–2359
15 Tran, Q.V., Chun, T.W., Ahn, J.R., Lee, H.H.: 'Algorithms for controlling both the DC boost and AC output voltage of Z-source inverter', *IEEE Trans. Ind. Electron.*, 2007, **54**, (5), pp. 2745–2750
16 Jung, J., Keyhani, A.: 'Control of a fuel cell based Z-source converter', *IEEE Trans. Ind. Electron.*, 2007, **22**, (2), pp. 467–476
17 Huang, Y., Shen, M.S., Peng, F.Z., Wang, J.: 'Z-source inverter for residential photovoltaic systems', *IEEE Trans. Power Electron.*, 2006, **21**, (6), pp. 1776–1782
18 Zhang, S., Tseng, K., Vilathgamuwa, D.M., Nguyen, T.D., Wang, X.: 'Design of a robust grid interface system for PMSG-based wind turbine generators', *IEEE Trans. Ind. Electron.*, 2011, **58**, (1), pp. 316–328
19 Zhou, Z.J., Zhang, X., Xu, P., Shen, W.X.: 'Single-phase uninterruptible power supply based on Z-source inverter', *IEEE Trans. Ind. Electron.*, 2008, **55**, (8), pp. 2997–3003
20 Gajanayake, C.J., Vilathgamuwa, D.M., Loh, P.C., Teodorescu, R., Blaabjerg, F.: 'Z-source-inverter-based flexible distributed generation system solution for grid power quality improvement', *IEEE Trans. Energy Convers.*, 2009, **24**, (3), pp. 695–704
21 Liu, Y., Ge, B., Abu-Rub, H., Peng, F.Z.: 'Control system design of battery-assisted quasi-Z-source inverter for grid-tie photovoltaic power generation', *IEEE Trans. Sustain. Energy*, 2013, **4**, (4), pp. 994–1001
22 Ge, B., Abu-Rub, H., Peng, F.Z., *et al.*: 'An energy-stored quasi-Z-source inverter for application to photovoltaic power system', *IEEE Trans. Ind. Electron.*, 2013, **60**, (10), pp. 4468–4481
23 Rocabert, J., Luna, A., Blaabjerg, F., Rodŕiguez, P.: 'Control of power converters in AC microgrids', *IEEE Trans. Power Electron.*, 2012, **27**, (11), pp. 4734–4739
24 Hamzeh, M., Karimi, H., Mokhtari, H.: 'A new control strategy for a multi-bus MV microgrid under unbalanced conditions', *IEEE Trans. Power. Syst.*, 2012, **27**, (4), pp. 2225–2232
25 Tremblay, O., Dessaint, L.A., Dekkiche, A.I.: 'A generic battery model for the dynamic simulation of hybrid electric vehicles'. Proc. IEEE Vehicle Power Propulsion Conf., TX, 2007, pp. 284–289
26 Kuo, Y.C., Liang, T.J., Chen, J.F.: 'Novel maximum-power-point tracking controller for photovoltaic energy conversion system', *IEEE Trans. Ind. Electron.*, 2001, **48**, (3), pp. 594–601